Journal of Materials Chemistry B

ROYAL SOCIETY OF CHEMISTRY

PAPER

View Article Online
View Journal | View Issue

Cite this: J. Mater. Chem. B, 2023, 11, 11319

Antibacterial, antioxidant and injectable hydrogels constructed using CuS and curcumin co-loaded micelles for NIR-enhanced infected wound healing†

Pengpeng Jia,[ab] Yu Zou *[ab] and Jiang Jiang *[ab]

Constructing antibacterial and antioxidant hydrogels is critical for treating infected full-thickness skin wounds. Herein, we report a co-encapsulation strategy to load CuS nanoparticles and hydrophobic antioxidant curcumin (cur) in aldehyde-terminated F127 micelles, which are then cross-linked with carboxymethyl chitosan through a Schiff base reaction to form a functional composite hydrogel (CF–CuS–cur). Apart from its suitable swelling and degradation behavior, good biocompatibility, and injectability for treating irregular wounds, the CF–CuS–cur hydrogel displayed excellent photothermal antibacterial ability under 1064 nm NIR laser irradiation, and antioxidant activity to protect cells from excessive oxidative stress. Using a full-thickness infected wound model, we demonstrated that the CF–CuS–cur hydrogel accelerated the wound healing process by effective sterilization and decreased inflammation, under synergistic action from CuS, curcumin and NIR irradiation. Histological and immunohistochemistry analysis further revealed the promoted skin attachments and regeneration, collagen deposition, neovascularization, and early transition to anti-inflammatory M2 macrophages, when the wounds were treated with the CF–CuS–cur hydrogel. This work demonstrates a facile strategy to construct functional hydrogels with NIR-enhanced antibacterial and antioxidant properties, which can be potentially applied as wound dressings for treating chronic wounds.

Received 29th September 2023,
Accepted 12th November 2023

DOI: 10.1039/d3tb02278a

rsc.li/materials-b

Introduction

Skin is the first physiological barrier of human beings, with the functions of defense, thermo-regulation, and signaling perception.[1,2] However, a volatile external environment may cause various damages to the skin, even threatening human life after the wounds get infected by pathogens such as *Staphylococcus aureus* (*S. aureus*),[3,4] as it may be difficult for the infected wounds to heal in a short time, due to possible secondary infection and chronic inflammation.[5] In response to pathogenic bacterial invasion, the infected wounds will recruit macrophages, neutrophils and other inflammatory cells, causing the appearance of acute inflammation, which is a protective response of the body to the injured wounds.[6] In general, balanced inflammation is beneficial for wound healing, because inflammatory cells have the ability to clean the wound by phagocytosing normal cell debris and bacteria.[7,8] However, uncontrolled inflammatory response and excessive reactive oxygen species (ROS) generation within the wound sites may also cause severe damage to endothelial cells and immune cells, which will significantly restrict angiogenesis and impede wound healing.[9,10] Therefore, it is essential to develop effective dressing materials for the timely resolution of sterilization, ROS scavenging and anti-inflammation, for wound healing applications.

Recently, copper sulfide nanoparticle (CuS NP) incorporated hybrid hydrogels have been demonstrated to be a potential dressing material for infected wound healing.[11–15] CuS NPs have displayed an excellent bactericidal effect under near-infrared (NIR) light irradiation, due to their superb photothermal properties.[15–18] The absorption maximum (normally ~ 1000 nm) of CuS NPs generally lies in the second NIR window, which could provide safer laser treatment, as the maximum permissible exposure to a 1064 nm laser (1 W cm^{-2}) is higher than that at 808 nm (0.33 W cm^{-2}), according to the American National Standard for Safe Use of Lasers (ANSI Z136.1–2007). Moreover, copper ions released from CuS NPs are also beneficial

[a] School of Nano-Tech and Nano-Bionics, University of Science and Technology of China, Hefei 230026, China. E-mail: yzou2012@sinano.ac.cn, jjiang2010@sinano.ac.cn
[b] i-Lab, CAS Key Laboratory of Nano-Bio Interface, Suzhou Institute of Nano-Tech and Nano-Bionics, Chinese Academy of Sciences, Suzhou 215123, China

† Electronic supplementary information (ESI) available: TEM and XRD of CuS, ^{1}H NMR of F127-CHO, TEM images and size distribution of micelles, hydrogel's pore sizes and gelation behavior, optical spectra of the hydrogels, cell viability in the presence of H_2O_2, and photographs showing injection of hydrogels to treat wounds. See DOI: https://doi.org/10.1039/d3tb02278a

for sterilization, which can cause bacterial death by destroying bacterial cytoderm and inducing cytoplasm degradation.[19] In addition, ample research data indicate that trace levels of copper ions will stimulate new blood vessel formation, and promote endothelial cell proliferation and migration.[20] Furthermore, by incorporating CuS NPs in the network of hydrogels, the potential copper dose toxicity can be avoided, and the overall biocompatibility was improved.[21] Despite the recent progress made in fabricating CuS nanocomposite hydrogels and their applications toward wound healing, there are scarcely any reports on improving their antioxidant and anti-inflammatory ability, which is also essential for enhanced infected wound healing.

In pursuit of finding efficient antioxidants to regulate overexpressed ROS and alleviate an uncontrolled inflammatory response, synthesized nanozymes have shown great potential in the treatment of high-inflammatory diseases.[22–24] In addition, natural extractives, such as tannic acid,[25] quercetin,[26] and curcumin,[27] have been discovered to exhibit inherent antioxidant and anti-inflammatory properties. Among them, curcumin (cur), a natural polyphenolic compound extracted from herb curcuma longa, exhibits a wide range of pharmacological activities, including antitumor, antimicrobial, antioxidant and anti-inflammatory effects.[28–30] Extensive research evidence has indicated that curcumin can effectively restrain the production of tumor necrosis factor-alpha (TNF-α), interleukin-1 beta (IL-1β) and other pro-inflammatory cytokines.[31] However, the feasibility and efficacy of curcumin are limited by its poor buffer solubility and uncontrolled drug release behavior.[32,33]

To overcome the limitations of hydrophobic drugs, various drug delivery systems based on amphipathic molecules have been developed.[34] In particular, Pluronic F127 (F127), an amphiphilic triblock copolymer consisting of hydrophilic polyethylene oxide (PEO) and hydrophobic polypropylene oxide (PPO) arranged in a A–B–A structure PEO_x–PPO_y–PEO_x,[35] can self-assemble into micelles in aqueous solution. Due to its biocompatibility and drug loading capacity both in the hydrophobic core and hydrophilic shell,[36] F127 has been approved by FDA for its application in hydrophobic drug delivery. Furthermore, various F127 derivatives including aldehyde-terminated F127 (F127-CHO), alkoxyamine-terminated F127 (F127-NH_2) and diacrylate F127 (F127-DA) have been used as both drug carriers and crosslinkers of hydrogels,[37] making F127 and its derivatives promising candidates to overcome the limitations of low curcumin delivery efficiency.

Herein, we prepared CuS NPs and curcumin co-loaded F127-CHO micelles (F127-CHO@CuS/cur) through an anti-solvent method, which simultaneously act as drug carriers, photothermal agents and crosslinkers for subsequent hydrogel formation. Carboxymethyl chitosan was used as the main framework molecule to crosslink with F127-CHO@CuS/cur micelles through a Schiff base reaction, thus forming CuS NPs and curcumin co-loaded hydrogel (CF–CuS–cur). The preparation process of nanocomposite micelles and the CF–CuS–cur hydrogel is schematically shown in Scheme 1. The F127-CHO@CuS/cur micelles not only acted as the crosslinking point to ensure adequate dispersion of curcumin in the hydrogel matrix, but also endowed the CF–CuS–cur hydrogel with a photothermal-controlled drug releasing capability. As a result, the CF–CuS–cur hydrogel exhibited excellent photothermal antibacterial ability under 1064 nm NIR laser irradiation, and antioxidant activity. Moreover, the CF–CuS–cur hydrogel showed a typical shear thinning properties, which makes it injectable and suitable for adequate adhesion to irregular wounds. Finally, using a full-thickness infected wound model, we demonstrated that the CF–CuS–cur hydrogel accelerated the wound healing process by effective sterilization and decreased inflammation within the wound microenvironment, corroborated by histological and immunohistochemistry analysis.

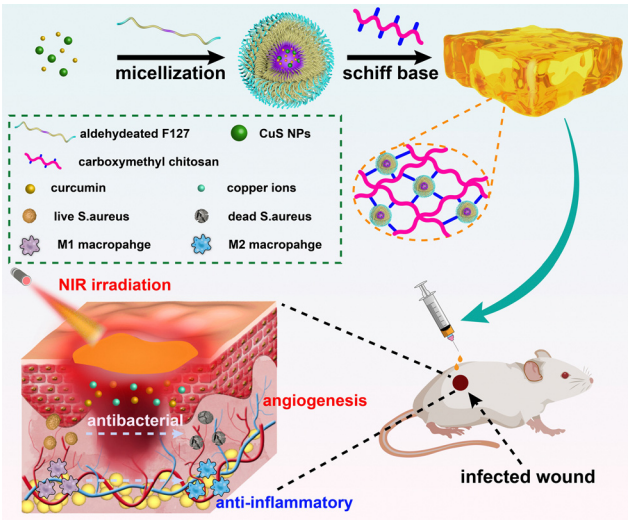

Scheme 1 Schematic illustration of the procedure for co-micellization of CuS NPs and curcumin with aldehyde-terminated F127, the formation of the CF–CuS–cur hydrogel and its application for infected full-thickness cutaneous wound healing.

Experimental section

Materials

Copper(II) chloride dihydrate ($CuCl_2{\cdot}2H_2O$, 99%), ammonium sulfide ($(NH_4)_2S$, 30–35%), iron sulfate heptahydrate ($FeSO_4{\cdot}7H_2O$), hydrogen peroxide (H_2O_2, 35%), potassium persulfate ($K_2S_2O_8$, 99.5%), toluene (C_7H_8, AR), dichloromethane (CH_2Cl_2, 99.5%), ethanol (C_2H_6O, 99.5%) and methanol (CH_4O, 99.5%) were bought from Sinopharm Chemical Reagent Co., Ltd. Pluronic F127 (F127), Dess–Martin periodinane ($C_{13}H_{13}IO_8$, 96%), curcumin ($C_{21}H_{20}O_6$, 98%), oleylamine ($C_{18}H_{35}N$, 98%), and thiazolyl blue tetrazolium bromide ($C_{18}H_{16}BrN_5S$, 98%) were obtained from Aladdin. Carboxymethyl chitosan (substitution: ≥80%), 3,3′,5,5′-tetramethylbenzidine ($C_{16}H_{20}N_2$, 99%), and 2,2′-azino-bis(3-ethylbenzothiazoline-6-sulfonic acid) diammonium salt ($C_{18}H_{24}N_6O_6S_4$, 99%) were purchased from Macklin. ROS assay kit and Calcein/PI live/dead viability/cytotoxicity assay kit were bought from Beyotime. The bacterial strains Gram-negative *Staphylococcus aureus* (*S. aureus*, ATCC-14458) and Gram-positive *Escherichia coli* (*E. coli*, ATCC-8739) were obtained from Luwei Microbial Sci&Tech Co, Ltd

(Shanghai, China). Human umbilical vein endothelial cells (HUVECs, Catalog. NO. #8000) were purchased from ScienceCell (Shanghai, China).

Preparation of aldehyde-terminated F127 (F127-CHO)

F127-CHO was prepared according to a previously published method with certain modifications.[38] 2.52 g of F127 (0.2 mmol) was dissolved in 200 mL of dichloromethane with a final concentration of 1 mM. Subsequently, 0.17 g of Dess–Martin periodinane was added into the above solution and ultrasonically dispersed to obtain a milky white solution. The reaction was conducted at 40 °C under continuous stirring. After 24 h, the reaction was stopped, with the solution filtered immediately to remove excess Dess–Martin periodinane, and the crude product was obtained after the solvent was completely evaporated. The product was then recrystallized three times with absolute ethanol to obtain the final F127-CHO.

Synthesis of CuS NPs

0.5 mmol $CuCl_2{\cdot}2H_2O$ was added in 10 mL of oleylamine and ultrasonically dissolved to obtain a homogeneous blue solution. Subsequently, 50 μL of $(NH_4)_2S$ was added into the above solution every 30 s until the volume of $(NH_4)_2S$ reaches 800 μL. Then, 20 mL of absolute ethanol was added to terminate the reaction. The mixture was then centrifuged and washed with dichloromethane and absolute ethanol to obtain CuS NPs. The CuS NPs were re-dispersed in dichloromethane, with a concentration of 5 mg mL^{-1}.

Synthesis of CuS NPs and curcumin co-loaded F127-CHO micelles (F127-CHO@CuS/cur)

The composite micelles were prepared according to the published study with some modifications.[39] Briefly, 1 g of F127-CHO was dissolved in 25 mL of dichloromethane with subsequent addition of 5 mL methanol containing 5 mg of curcumin. Then, the above mixture was placed under constant stirring, with the addition of 1 mL of CuS NPs solution (5 mg mL^{-1}) at room temperature. After 1 h, the mixture was condensed with a rotary evaporator at 50 °C. Thus the obtained product was re-dispersed in 20 mL of H_2O at room temperature with continuous stirring to ensure the micellization, followed by freeze drying to obtain a F127-CHO@CuS/cur sponge. Finally, the F127-CHO@CuS/cur sponge was dispersed in H_2O to form a 20% solution, which was used throughout the following study. Separately, curcumin loaded F127-CHO micelles (F127-CHO@cur) or CuS NPs loaded F127-CHO micelles (F127-CHO@CuS) were prepared following the same procedures, except with the addition of either curcumin solution or CuS NP solution only.

Preparation of CuS NPs and the curcumin co-loaded hydrogel (CF–CuS–cur)

The CF–CuS–cur hydrogel was prepared using a Schiff base crosslinking method. In brief, 10% carboxymethyl chitosan aqueous solution was mixed with 20% F127-CHO@CuS/cur micelles at a fixed volume ratio (3 : 1), and then placed at room temperature for 1 h to obtain CF–CuS–cur hydrogel. A curcumin loaded hydrogel (CF–cur) or CuS NP loaded hydrogel (CF–CuS) was prepared following the same procedures, by adding only F127-CHO@cur or F127-CHO@CuS micelles.

Physiochemical evaluation of the CF–CuS–cur hydrogel

The swelling (fluid absorbing) ability of the hydrogel was examined by placing 500 μL of CF–CuS–cur hydrogel in a 5 mL vial with subsequent addition of 3 mL PBS. Then, the vial containing hydrogel was photographed at 0, 4, 12, and 24 h and weighed after discarding PBS. The water absorbing rate was calculated according to the following equation:

$$\text{water absorbing rate} = \frac{W_t - W_0}{W_0} \times 100\% \quad (1)$$

where W_0 and W_t represent the weight of the initial CF–CuS–cur hydrogel and the weight of the absorbing hydrogel after specific time points.

To evaluate its degradation behavior, 500 μL of CF–CuS–cur hydrogel was completely frozen, weighed and socked in 10 mL PBS at 37 °C under mild stirring. Subsequently, the hydrogel was taken out and completely frozen to obtain the weight at 0, 4, 12, 24, 72, and 120 h, respectively. The degradation behavior was evaluated based on the remaining weight of the CF–CuS–cur hydrogel and calculated based on the following equation:

$$\text{degradation rate} = \frac{W_t}{W_0} \times 100\% \quad (2)$$

where W_0 and W_t represent the weight of the dried CF–CuS–cur hydrogel at 0 h and t h, respectively.

The rheology and viscosity of the hydrogel were investigated using a RS6000 rotational rheology analyzer (HAAKE, Germany). For rheological measurements, 70 μL of CF–CuS, CF–cur or CF–CuS–cur hydrogels were added onto the center of the test platform (diameter: 20 mm), with the thickness set to 0.2 mm. The sweep frequency range was 0.1–10 Hz in oscillating frequency mode. The viscosity was measured under shear thinning mode with the shearing rate of 0.1–200 S^{-1}, and the sample preparation was the same as that in the rheological experiment.

In vitro antioxidant ability of the CF–CuS–cur hydrogel

3,3′,5,5′-Tetramethylbenzidine (TMB) was selected as the hydroxyl radical (•OH) probe, for colorimetric evaluation of •OH scavenging efficiency.[40] 10 μL of H_2O_2 (50 mM) was added into 1 mL of $FeSO_4$ aqueous solution (0.1 mM), followed by immediate addition of 0, 20, 60, and 100 μL of CF–CuS–cur hydrogel. Subsequently, 1 mL of TMB aqueous solution (0.6 mM) was added into the above solution mixture. After 10 min incubation in the dark, the solution absorbance at 650 nm was measured using a UV-vis-NIR spectrometer.

2,2′-Azino-bis(3-ethylbenzothiazoline-6-sulfonic acid) diammonium salt radical (ABTS•) was used to evaluate the total antioxidant capacity of the CF–CuS–cur hydrogel based on colorimetric analysis. Briefly, 5 mL of ABTS aqueous solution (7 mM) was mixed with 5 mL of potassium persulfate (KPS)

aqueous solution (2.45 mM) for 16 h while keeping away from light, to obtain the dark blue ABTS$^{\bullet}$ solution. Then, different amounts of the CF–CuS–cur hydrogel (0, 10, 30, 50 μL) were separately added into 1 mL ABTS$^{\bullet}$ solution that was diluted 10 times beforehand. After incubating for 10 min in the dark, the absorbance of the solution mixture at 731 nm was recorded on a UV-vis-NIR spectrometer.

Photothermal properties of the CF–CuS–cur hydrogel

100 μL of CF–CuS–cur hydrogel was added into 96-well plates and irradiated with 1064 nm NIR light for 10 min at different power densities (0.25, 0.50, 0.75, and 1.00 W cm^{-2}). During the illumination period, the hydrogel surface temperature was monitored and imaged every minute using an infrared thermal camera. The photothermal conversion efficiency (η) of the CF–CuS–cur hydrogel was calculated based on the following equations, with data acquired from the corresponding heating and cooling curves:

$$\eta = \frac{hS(T_{max} - T_{surr}) - hS(T_{max,water} - T_{surr})}{I(1 - 10^{-A_{1064}})} \quad (3)$$

$$\theta = \frac{\Delta T}{\Delta T_{max}} = \frac{T - T_{max}}{T_{max} - T_{surr}} \quad (4)$$

$$\tau_s = \frac{m_d c_d}{hS} \quad (5)$$

where h represents the heat transfer coefficient, S is the exposed surface of the CF–CuS–cur hydrogel, T_{max} is the maximum equilibrium temperature under NIR laser irradiation, T_{surr} stands for the ambient temperature, A_{1064} represents the absorbance of the CF–CuS–cur hydrogel with fixed thickness at 1064 nm, I is the used NIR laser power density, τ_s represents the thermal time constant based on the plot of $-\ln(\theta)$ *vs.* time, m_d is the weight of the CF–CuS–cur hydrogel and c_d is the specific heat capacity of water (4.2 J g^{-1} K^{-1}).

In vitro curcumin release

The standard calibration curve was first established according to the measured optical absorbance of curcumin solutions at 426 nm with known concentrations. Then, 500 μL of CF–CuS–cur hydrogel was added into a 10 mL tube, followed by subsequent addition of 5 mL PBS, and the tube was placed in a 37 °C bath under mild stirring. 1 mL of supernatant was taken out at 0, 4, 12, 24, 48, 72, 96, and 120 h, with equal volume of fresh PBS re-supplemented into the tube. The respective absorbance values of aliquots at 426 nm were measured to determine the corresponding curcumin concentration, and the cumulative curcumin release rate was acquired by fitting the release curve with a Higuchi equation. The influence of photothermal effect on curcumin release behavior was investigated by alternating NIR laser irradiation (0.75 W cm^{-2}, laser on for 5 min followed by off for 5 min, 30 min total).

In vitro antibacterial assays

For the evaluation of *in vitro* antibacterial performance, experiments were conducted on ten parallel groups: (1) control (blank), (2) control +, (3) CF hydrogel, (4) CF hydrogel +, (5) CF–CuS hydrogel, (6) CF–CuS hydrogel +, (7) CF–cur hydrogel, (8) CF–cur hydrogel +, (9) CF–CuS–cur hydrogel, and (10) CF–CuS–cur hydrogel +. The + sign indicates NIR laser irradiation (1064 nm, 0.75 W cm^{-2}, 10 min). *E. coli* or *S. aureus* (10^7 CFU per mL, 100 μL) during the logarithmic growth phase was placed on the surface of the hydrogel, which was added beforehand in 24-well plates (500 μL per well). For the groups with light irradiation, NIR light was applied for 10 min, followed by culturing for 50 min. The bacteria of the groups without light treatment were co-cultured with the hydrogel for 1 h. After that, 1 mL of PBS was added to form a bacteria diluent, and 50 μL of this diluted solution was spread onto agar dishes with subsequent incubation for 16 h at 37 °C. The bacterial colonies on the dishes were photographed by camera and analyzed by ImageJ.

Scanning electron microscopy (SEM) was used to investigate the morphological characteristics of *E. coli* and *S. aureus* after *in vitro* antibacterial treatments. Briefly, 1 mL of *E. coli* or *S. aureus* suspension during the logarithmic growth phase (OD = 0.7) was precipitated by centrifugation at 5000 rpm for 10 min, and re-dispersed into 100 μL PBS to obtain a condensed bacteria suspension. After the above-described antibacterial treatments, the bacteria suspension was collected and fixed with 4% paraformaldehyde overnight at 4 °C. The fixed bacteria were washed by PBS and dehydrated with different concentrations of ethanol solutions (50%, 75%, 95%, 100%) in sequence. Finally, the bacteria samples were dropped onto pieces of silicon substrates, which were sprayed with gold before SEM measurement.

In vitro cell cytotoxicity and hemolysis assays

Human umbilical vein endothelial cells (HUVECs) were seeded in 24-well plates (5×10^4 cells per well) and cultured overnight. Subsequently, the CF hydrogel, CF–CuS hydrogel, CF–cur hydrogel and CF–CuS–cur hydrogel of a series of concentrations (2, 4, 6, 8, 10 μL mL^{-1}) were added into the corresponding wells. Wells without any hydrogel addition were set as the control group. After incubating for 24 h, MTT assay was conducted and the cell viability was determined based on the absorbance of each well at 495 nm measured using a microplate reader.

The live/dead staining assay was used to evaluate the cell viability visually. HUVECs were seeded in 24-well plates (5×10^4 cells per well) and cultured overnight. The CF hydrogel, CF–CuS hydrogel, CF–cur hydrogel and CF–CuS–cur hydrogel were added into the corresponding wells with a fixed concentration (10 μL mL^{-1}). After incubating for 24 h, HUVECs were stained with Calcein-AM and PI for 15 min. The stained cells were then washed with PBS and imaged under an inverted fluorescence microscope.

For hemolysis evaluation, erythrocytes from a Sprague Dawley (SD) rat were isolated by centrifugation at 3000 rpm

for 5 min, which were then diluted to 5% (v/v) with PBS after washing three times. 500 μL of CF hydrogel, CF–CuS hydrogel, CF–cur hydrogel and CF–CuS–cur hydrogel were added in 24-well plates, and incubated with 1 mL of diluted erythrocyte suspension at 37 °C with mild shaking (100 rpm). PBS and deionized water were taken as the negative and positive controls, respectively. After 1 h, the diluted erythrocyte suspension of each group was collected and centrifuged. The corresponding absorbance at 540 nm of the suspension was measured using a UV-vis-NIR spectrometer, to calculate the hemolysis ratio:

$$\text{hemolysis ratio} = \frac{A_t - A_n}{A_p - A_n} \times 100\% \quad (6)$$

where A_t, A_n and A_p represent the absorbance at 540 nm of the corresponding experimental group, negative control group and positive control group, respectively.

In vitro cell antioxidant evaluation

Following a previously reported method,[41] the antioxidant properties of curcumin containing CF–cur hydrogel or CF–CuS–cur hydrogel were assessed by evaluating the viability of HUVECs under a high H_2O_2 concentration environment. 1 mL of HUVECs (2×10^5 cells per well) were seeded in 24-well plates and cultured overnight. Each well was then added with 10 μL of high concentration H_2O_2 (400 mM) and 10 μL of CF–cur hydrogel or CF–CuS–cur hydrogel. HUVECs cultured without any additives and only with H_2O_2 were set as negative and positive controls, respectively. After incubating for 5 h, MTT assay and DCFH-DA staining were separately conducted to evaluate the cell viability and the total cellular oxidative stress.

In vivo full-thickness infected wound healing

The full-thickness infected wound model of SD rats (female, ~220 g, 6–7 weeks, Henan Skbex Biotechnology Co., Ltd) was constructed for wound healing experiments. All the animal experiments were approved by the Animal Ethics Committee of Suzhou Institute of Nano-Tech and Nano-Bionics, Chinese Academy of Sciences (SINANO/EC/2023-038). Briefly, SD rats were randomly divided into five experimental groups: (1) control, (2) CF hydrogel, (3) CF–CuS hydrogel +, (4) CF–cur hydrogel and (5) CF–CuS–cur hydrogel + (+ represents 1064 nm laser irradiation, 0.75 W cm^{-2}, 10 min). All rats were intraperitoneally injected with 7% chloral hydrate solution (0.6 mL/100 g), and the back of rat was depilated with 8% sodium sulfide solution. Sterile shear was used to create approximately rounded wounds (diameter: ~10 mm, thickness: ~2 mm). Subsequently, *S. aureus* (10^6 CFU per mL, 100 μL) during the logarithmic growth phase was used to infect the wounds. Finally, different hydrogels (~ 200 μL) were applied onto the corresponding wounds. An infrared thermal camera was used to monitor and record the temperature changes of wound sites from the irradiation groups. The wounds were photographed by a camera on day 0, 3, 7, 11, and 14, with the respective wound areas were analyzed by ImageJ.

Histological and immunohistochemistry analysis

Euthanasia was applied to rats before obtaining their wound skin tissue samples after various treatments, which were then fixed with 4% paraformaldehyde. Every sample was processed into slices for hematoxylin-eosin (H&E) and Masson staining. Furthermore, immunohistochemistry staining (CD31 and CD206 expression) was carried out at predetermined time points (day 7 and day 14) according to standard protocols.

Statistical analysis

All experimental data were statistically analyzed using at least three individual samples and presented as the mean ± standard deviation (mean ± SD). One-way ANOVA following the Bonferroni post-hoc test was performed to determine the statistical differences using Origin. Statistical significance was set at: $*p < 0.05$, $**p < 0.01$, and $***p < 0.001$.

Results and discussion

Preparation of CF–CuS–cur hydrogel

We first synthesized CuS NPs in the organic phase based on previously reported procedures.[42] The CuS NPs thus obtained were in irregular shapes, with average nanoparticle sizes of about 7 nm (ESI,† Fig. S1a). The powder X-ray diffraction (XRD) pattern (Fig. S1b, ESI†) indicates these CuS NPs were in covellite phase (PDF #06-0464). F127 was then chosen as the carrier for the co-loading of hydrophobic curcumin and CuS NPs. To allow for the subsequent hydrogel formation *via* cross-linking through Schiff base reaction, we modified F127 with terminal aldehyde groups (F127-CHO), by oxidizing the terminal hydroxyl of F127 using Dess–Martin periodinane. As shown in Fig. S2 (ESI†), the ^1H NMR spectrum shows a new peak emerged at 9.7 ppm, corresponding to the protons of newly formed terminal aldehyde groups, which indicates the successful synthesis of F127-CHO.[38,43]

Then, three kinds of F127-CHO micelles were prepared using an anti-solvent method: CuS NP loaded micelles (F127-CHO@CuS), curcumin loaded micelles (F127-CHO@cur), as well as CuS NPs and curcumin co-loaded micelles (F127-CHO@CuS/cur), with respective loading capacities of 0.228 mg g^{-1} for CuS and 0.224 mg g^{-1} for curcumin. The TEM image in Fig. 1a shows that F127-CHO@CuS/cur micelles were spherical with overall sizes less than 100 nm. Due to the rather small size of CuS NPs, a bright-field TEM image was unable to clearly identify the CuS NPs inside the F127 micelles. Nevertheless, the HAADF-STEM image reveals the distinct contrast of CuS NPs (the inset in Fig. 1a). The average size of F127-CHO@CuS/cur micelles was determined to be 67.4 ± 6.0 nm (Fig. 1b), and their dispersion was chartreuse in color with an obvious Tyndall effect (inset photographs in Fig. 1b). F127-CHO@CuS micelles (Fig. S3a and b, ESI†) have similar shape and particle size (61.8 ± 13.4 nm) to F127-CHO@CuS/cur micelles, while F127-CHO@cur micelles (Fig. S3c and d, ESI†) show an apparent difference in shape and particle size (33.0 ± 7.2 nm) compared with the other two kinds of micelles, which may be

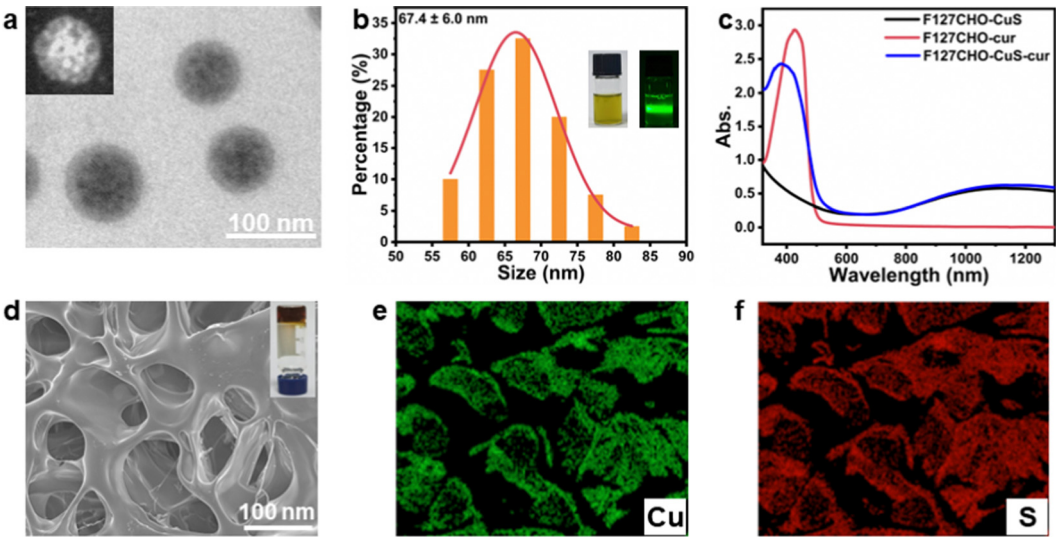

Fig. 1 (a) The TEM image of F127-CHO@CuS/cur micelles (inset: HADDF-STEM image of a single micelle); (b) statistical size distribution of F127-CHO@CuS/cur micelles (inset: photograph of the F127-CHO@CuS/cur aqueous solution and the Tyndall phenomenon); (c) UV-vis-NIR spectra of the F127-CHO@CuS, F127-CHO@cur, and F127-CHO@CuS/cur micelles; (d) the SEM image of CF–CuS–cur hydrogel (inset: photograph of the hydrogel) and the elemental mapping images for (e) Cu and (f) S.

ascribed to the absence of CuS NPs. Because of the co-loading of CuS NPs and curcumin, F127-CHO@CuS/cur micelles displayed both the broad near-infrared absorption (900–1300 nm) from CuS and the characteristic absorption peak at ~400 nm origination from curcumin (Fig. 1c).

Carboxymethyl chitosan is a chitosan derivative that has better water solubility and bioactivity, which is broadly used in drug delivery and tissue engineering.[44] It bears amino groups that can react with aldehyde groups in F127-CHO to form hydrogel *via* Schiff base reaction. In order to avoid the inherent physical self-gelation of F127-CHO aqueous solution with concentrations higher than 25% at room temperature (Fig. S4a, ESI†), we chose to use 20% F127-CHO aqueous solution and 10% carboxymethyl chitosan aqueous solution as the hydrogel precursors. The hydrogel formed immediately when the two precursors were mixed together with a volume ratio of 3 : 1 (Fig. S4b, ESI†). The corresponding hydrogels formed by mixing 10% carboxymethyl chitosan aqueous solution with 20% F127-CHO@CuS, F127-CHO@cur or F127-CHO@CuS/cur micelles solution were denoted as CF–CuS, CF–cur and CF–CuS–cur hydrogels, respectively. The three hydrogels all have relatively irregular pores (Fig. 1d and Fig. S5a, b, ESI†), with pore sizes at 81.6 ± 19.3, 48.1 ± 9.8, and 76.0 ± 16.5 μm (Fig. S5c, ESI†), respectively. The incorporation of CuS NPs leads to the formation of not only larger F127-CHO@CuS and F127-CHO@CuS/cur micelles, but also apparently increased hydrogel pore sizes. The elemental mapping images reveal that CuS NPs were evenly distributed inside the hydrogel matrix (Fig. 1e and f).

Mechanical, water absorbing and degradation properties of CF–CuS–cur hydrogel

Rheological analysis was used to evaluate the mechanical properties of the three hydrogels. As shown in Fig. 2a, the storage moduli (G') of all three hydrogels were obviously higher than the corresponding loss moduli (G''), with no intersections between G' and G'' upon progressively increasing the frequency from 0.1 to 10 Hz. This indicates that all three hydrogels possessed elastic-dominant properties, and the addition of different micelles did not induce distinct moduli change between hydrogels.

Subsequently, the static shear rate sweep was used to measure the viscosity of hydrogels (Fig. 2b). Three hydrogels all exhibited a steady decrease in viscosity with increasing shear rate, which means they have shear-thinning properties, likely due to the reversible dynamic Schiff base covalent bonding.[38] Furthermore, CF–CuS–cur hydrogel showed higher viscosity (~1400 Pa s) than CF–CuS and CF–cur hydrogel (515 and 201 Pa s, respectively). At a low shear rate (0.3–1 s^{-1}), the CF–CuS–cur hydrogel showed higher shear viscosity than that of CF–CuS and CF–cur hydrogels. However, CF–CuS–cur hydrogel displayed lower shear viscosity when the shear rate was higher (10–100 s^{-1}), suggesting its suitability to be used as an injectable hydrogel. Photographs shown in Fig. 2c give a better-visualized demonstration of the highly viscous and injectable properties of CF–CuS–cur hydrogel.

CF–CuS–cur hydrogel has a porous structure that can absorb the wound exudate, reduce the risk of infection and accelerate wound healing. Hence, the absorbing ability was evaluated by measuring the swelling rate of the hydrogels. As shown in Fig. 2d, CF–CuS–cur hydrogel showed a rapid absorbing ability within the first 4 h and then reached the equilibrium state. After 24 h, the CF–CuS–cur hydrogel absorbed ~54% water relative to its initial weight. Moreover, as depicted by the photographs in Fig. 2e, the boundary change between PBS and CF–CuS–cur hydrogel over time clearly shows the swelling behavior of the hydrogel. For practical applications, it is desirable to have the hydrogel with suitable degradation behavior. As shown in Fig. 2f, the CF–CuS–cur hydrogel lost more than

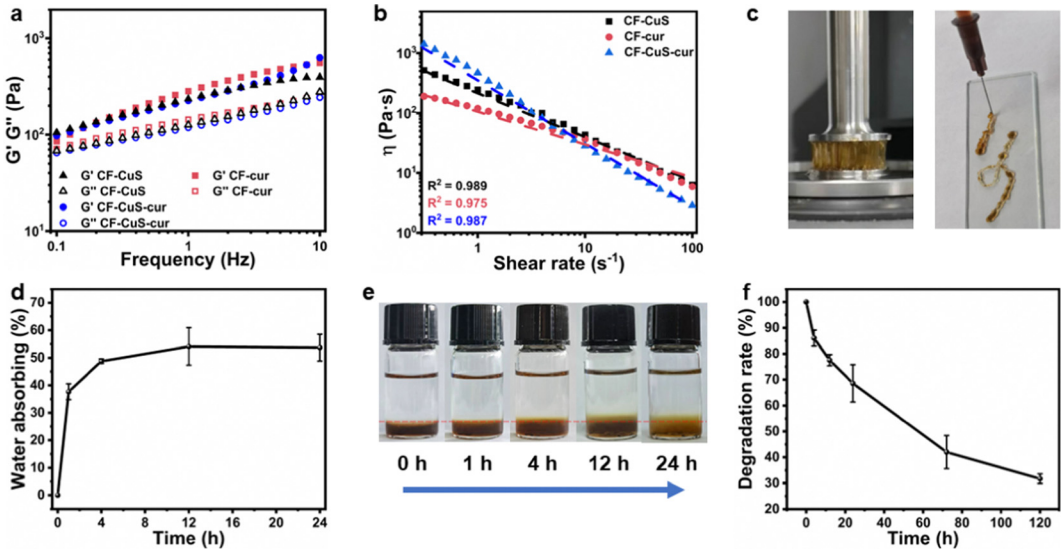

Fig. 2 (a) The rheological behavior (conducted by frequency sweep mode at a constant strain of 1%), and (b) viscosity as a function of shear rate for CF–CuS, CF–cur and CF–CuS–cur hydrogels; (c) photographs showing the highly viscous and injectable nature of CF–CuS–cur hydrogel; (d) water absorbing ability of CF–CuS–cur hydrogel, and (e) the corresponding photographs of the hydrogel soaked in PBS over time; (f) the degradation behavior of CF–CuS–cur hydrogel.

30% of its initial weight within 24 h, with only about 30% of the initial weight remaining after 5 days. These results manifest the good biodegradation characteristics of CF–CuS–cur hydrogel.

Photothermal and ROS scavenging properties of CF–CuS–cur hydrogel

As the CuS NPs and curcumin were encapsulated in F127 micelles before forming hydrogels, the CF–CuS–cur hydrogel retained the characteristic optical absorption from both CuS NPs in the NIR and curcumin in the ~400 nm region (Fig. S6, ESI†). Given that CuS NPs are strong NIR photothermal heating agents, the photothermal property of CF–CuS–cur hydrogel was investigated under 1064 nm laser irradiation with varying light intensity and illumination duration. As shown in Fig. 3a and b, the equilibrium surface temperature of CF–CuS–cur hydrogel rose to 34.8, 42.1, 52.1 and 59.5 °C at the end of 10 min illumination, with the corresponding laser power densities of 0.25, 0.50, 0.75 and 1.00 W cm^{-2}, respectively. Moreover, when CF–CuS–cur hydrogel was subjected under three laser on/off cycles of irradiation (at the power density of 0.75 W cm^{-2}), the same heating/cooling curves with no distinct temperature drop were observed (Fig. 3c), manifesting the good photothermal stability of CF–CuS–cur hydrogel. From the photothermal heating and cooling profile, the photothermal conversion efficiency (η) of CF–CuS–cur hydrogel was calculated to be 44.6%, according to eqn (3)–(5) shown in the Experimental section, with the fitting time constant shown in Fig. 3d.

Given that curcumin bears the antioxidant function, its release behavior from CF–CuS–cur hydrogel was then investigated. According to the standard calibration curve shown in Fig. 4a, curcumin was released slowly from CF–CuS–cur hydrogel under near physiological conditions (PBS, 37 °C), and the cumulative release reached ~25% after 120 h (Fig. 4b). This continuous

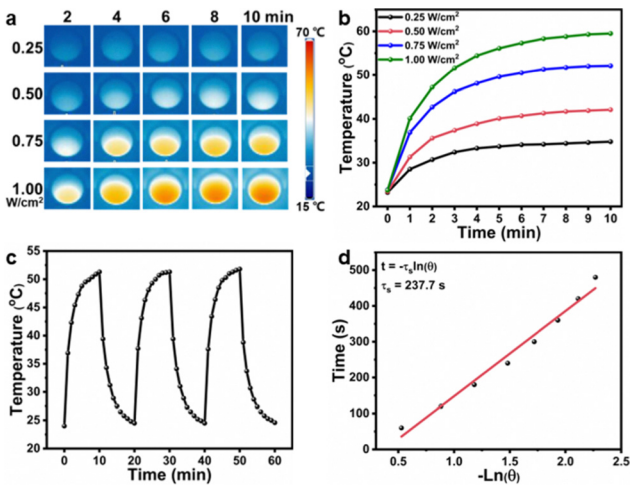

Fig. 3 (a) The infrared thermal images of CF–CuS–cur hydrogel after different irradiation durations under a 1064 nm laser with different power densities; (b) the corresponding temporal temperature elevation curves during the 10 min laser irradiation at different laser power densities; (c) the heating/cooling curves of the CF–CuS–cur hydrogel with three on/off irradiation cycles (1064 nm, 0.75 W cm^{-2}, 10 min for both on and off states); (d) the plot of cooling time *versus* the negative natural logarithm of the driving force temperature during the cooling phase.

slow-release behavior of curcumin can be beneficial for alleviating the oxidative stress and inflammation at the wound sites. Furthermore, due to the excellent photothermal property of CuS NPs, which was co-loaded in F127-CHO micelles with curcumin, applying NIR irradiation should be able to expedite the curcumin release rate. As shown in Fig. 4c, curcumin release from the CF–CuS–cur hydrogel was clearly accelerated upon turning on the laser irradiation at time = 5, 15, and 25 min, and slowed down when the laser was shut off at time = 10 and 20 min.

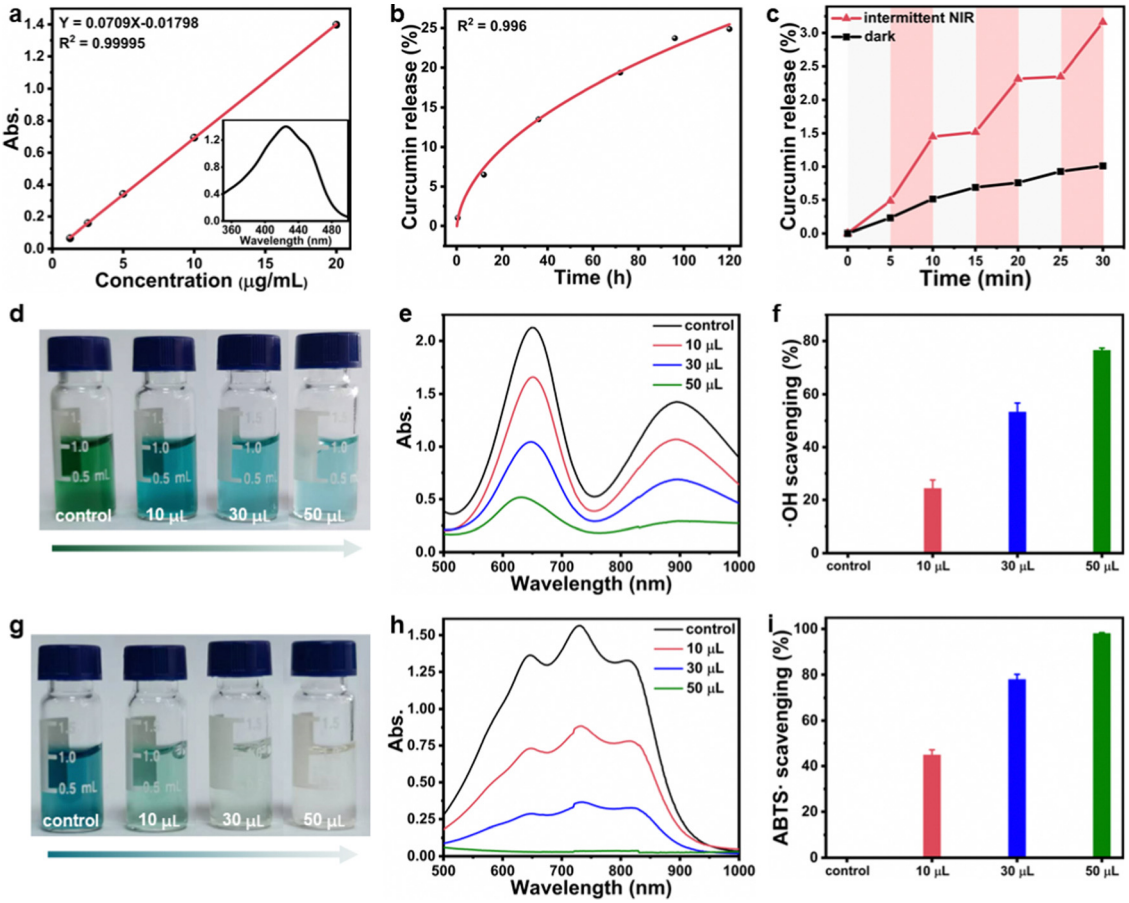

Fig. 4 (a) The standard calibration curve of curcumin with different known concentrations (inset: the UV-vis spectrum of curcumin); (b) curcumin release profile from the CF–CuS–cur hydrogel over 5 days under a simulated physiological environment (PBS, 37 °C); (c) curcumin release profile from CF–CuS–cur hydrogel in the dark, and under intermittent NIR irradiations (1064 nm, 0.75 W cm^{-2}); (d) the photographs of oxTMB solution after incubating with different amounts of CF–CuS–cur hydrogel, (e) the corresponding solution UV-vis-NIR spectra, and (f) the quantitative analysis of •OH scavenging percentages; (g) the photographs of ABTS• solution after incubating with different amounts of CF–CuS–cur hydrogel, (h) the corresponding solution UV-vis-NIR spectra, and (i) the quantitative analysis of ABTS• scavenging percentages. Data were expressed as mean ± SDs (n = 3).

For comparison, the curcumin release profile of CF–CuS–cur hydrogel in the dark was also plotted, displaying a slow but monotonically increased release profile. The intermittent NIR radiation resulted in more than three times of curcumin release after 30 min, compared to that under dark conditions. The photothermally enhanced curcumin release could be due to the following reasons: firstly, photothermal induced local heating may weaken the hydrophobic interactions between curcumin and F127, and accelerate curcumin desorption and diffusion out to the wound microenvironment;[45] secondly, due to their inherent thermos-sensitive characteristic, F127 micelles can experience slight shrinkage at elevated temperatures,[46] thus facilitating the release of curcumin. The above results demonstrate that curcumin release from CF–CuS–cur can be controlled and expedited by NIR light.

After establishing that curcumin can be released from CF–CuS–cur hydrogel, we went further to investigate its antioxidant property. 3,3′,5,5′-tetramethylbenzidine (TMB) was chosen as the detection probe of •OH, because •OH can oxidize colorless TMB into blue oxTMB, which can be then quantitatively analyzed using a simple colorimetric method. In an intentionally created •OH rich solution using H_2O_2 and $FeSO_4$ (detailed procedures in the Experimental section), TMB was quickly oxidized to oxTMB, forming a dark colored solution (photograph in Fig. 4d). Upon the addition of CF–CuS–cur hydrogel, the TMB solution color became lighter with increasing amount of added hydrogel, indicating CF–CuS–cur hydrogel can scavenge •OH in the solution, thus inhibiting the oxidation of TMB. The corresponding UV-vis-NIR spectra also show the progressively reduced characteristic absorption of oxTMB at 650 nm (Fig. 4e). By comparing the relative changes of oxTMB absorption at 650 nm, the •OH scavenging ability of CF–CuS–cur hydrogel was quantitatively evaluated (Fig. 4f). Specifically, the •OH scavenging capability reached 76% (calculated based on the ratio of the attenuated absorption value to the absorption value of the control group at 650 nm) with the addition of 50 μL CF–CuS–cur hydrogel. Furthermore, we used 2,2′-azino-bis(3-ethylbenzothiazoline-6-sulfonic acid) diammonium salt (ABTS) as another probe to evaluate the total antioxidant capacity of CF–CuS–cur hydrogel. By firstly oxidizing colorless ABTS to

a blue colored reactive nitrogen species (RNS, $ABTS^{\bullet}$) using potassium persulfate, followed by measuring the solution absorption in the presence and absence of CF–CuS–cur hydrogel, the antioxidant effect can be quantified by simply monitoring the colorimetric change at 731 nm, which originates from $ABTS^{\bullet}$. The $ABTS^{\bullet}$ solution color faded after adding various amounts of CF–CuS–cur hydrogel (Fig. 4g), demonstrating its effective antioxidant activity. By quantitatively analyzing the relative changes of $ABTS^{\bullet}$ absorption at 731 nm, the antioxidant ability of CF–CuS–cur hydrogel was quantitatively evaluated (Fig. 4h). By adding 50 μL CF–CuS–cur hydrogel into the $ABTS^{\bullet}$ solution, its characteristic absorption peak at 731 nm disappeared almost completely, corresponding to an $ABTS^{\bullet}$ scavenging percentage near 98% (Fig. 4i), manifesting the excellent antioxidant capability of CF–CuS–cur hydrogel.

In vitro antibacterial activity of CF–CuS–cur hydrogel

Encouraged by the excellent photothermal property of the CF–CuS–cur hydrogel, its *in vitro* antibacterial ability was then determined by using an agar plate counting method. *E. coli* and *S. aureus* were used as the model Gram-negative and Gram-positive bacteria strains, which were treated by hydrogel samples with (+) or without (−) NIR irradiation. As shown in Fig. 5a–d, NIR irradiation alone had no obvious influence on the two different types of bacteria strains (control group), as the bacterial colonies displayed almost no difference. As for CF hydrogel (hydrogel with neither CuS nor curcumin), it displayed no obvious antibacterial activity, even with NIR irradiation. In stark contrast, both CF–CuS and CF–CuS–cur hydrogel displayed strong NIR irradiation dependent antibacterial activity. The bacteria survival rate for the CF–CuS and CF–CuS–cur hydrogel group under NIR irradiation was only 1.0 ± 0.3%, 0.4 ± 0.3% for *E. coli* and 0.6 ± 0.3%, 0.2 ± 0.3% for *S. aureus*, respectively. While in the absence of NIR irradiation, CF–CuS hydrogel and CF–CuS–cur hydrogel only exhibited weak antibacterial ability, and the bacterial survival rate was 73.2 ± 2.8%, 67.2 ± 1.3% for *E. coli* and 75.7 ± 1.9%, 73.0 ± 0.3% for *S. aureus*, respectively, likely due to the presence of CuS NPs inside the hydrogel and the released copper ions.[12] The greatly enhanced antibacterial activity of the CuS NPs containing hydrogels (CF–CuS and CF–CuS–cur hydrogel) under NIR irradiation is because CuS NPs can effectively convert NIR light into local heat, thus destroying the enzymes and proteins of bacteria and causing bacterial death.[47] In comparison, CF–cur hydrogel displayed a weak bactericidal effect against both *E. coli* and *S. aureus*, regardless of the irradiation conditions. This could be due to the low level of curcumin release, despite its known intrinsic antibacterial activity.[48,49]

In order to determine the influence of different treatments on the morphologies and membrane integrity of the two bacteria strains, we used SEM to image the bacteria from the various experimental groups. As can be seen from Fig. 5e, *E. coli* have typical full rod-like structures with a clear surface and intact cell membrane, while *S. aureus* present approximately spherical structures with a smooth surface and intact morphologies (Fig. 5f) in the control group. The NIR irradiation under current experimental settings would not induce any damage to both *E. coli* and *S. aureus*. Similar bacterial morphologies were observed from CF hydrogel groups, with or without NIR irradiation, consistent with the observed lack of antibacterial activity on CF hydrogel. Similar observations were made for the CF–cur hydrogel group. However, distinct morphological changes and even membrane disruption were observed in the CF–CuS + NIR and CF–CuS–cur + NIR groups. These results demonstrate that local hyperthermia produced by CuS NPs under NIR irradiation can significantly cause bacteria membrane wrinkle, disruption and further leakage of inner content. These SEM measurements reveal that the excellent antibacterial activity of CF–CuS–cur hydrogel under NIR irradiation was due to photothermal induced bacteria structure disruption.

Biocompatibility and antioxidant properties of CF–CuS–cur hydrogel

Biocompatibility is the crucial property for antibacterial materials in the biomedical field. The cytotoxicity of the different hydrogels under normal conditions was evaluated using Human Umbilical Vein Endothelial Cells (HUVECs). Live/dead staining was conducted to give a visual presentation of the cytocompatibility. As shown in Fig. 6a, due to slight differences in the initial cell seeding, apparent cell densities varied a little among different groups. Nevertheless, the fluorescence images of all groups showed that most of the HUVECs are stained with green fluorescing Calcein but not the red fluorescent PI, manifesting the cells were mostly alive. Independent MTT assays were also conducted to obtain the quantitative analysis of HUVECs viability, which revealed negligible cytotoxicity of the various hydrogels (Fig. 6b). Furthermore, hemolysis assay was also performed to evaluate the blood compatibility of CF–CuS–cur hydrogel (Fig. 6c). Distinct differences were observed between the red supernatant of the positive control (DI water), and the pale yellow supernatant from the CF–CuS–cur hydrogel and other hydrogel groups, with the specific hemolysis ratio calculated to be below 5%. Both cytotoxicity and hemolysis assays have demonstrated the good biocompatibility of CF–CuS–cur hydrogel.

Building on the results of solution ROS scavenging ability of CF–CuS–cur hydrogel, we went further to study the protective effect of the CF–CuS–cur hydrogel on cells in a highly oxidative environment. For this study, HUVECs were first cultured in media with excessive H_2O_2 (100, 200, 300, 400 μM) for 5 h, and the cell survival rate decreased with increasing H_2O_2 concentration, with less than 40% of HUVECs surviving in the presence of 400 μM H_2O_2 (Fig. S7, ESI†). Hence, 400 μM H_2O_2 was picked for comparative study, and we added CF–cur hydrogel or CF–CuS–cur hydrogel into the cultured environment of HUVECs that was spiked with 400 μM H_2O_2. Furthermore, a ROS probe DCFH-DA was used to stain the intracellular ROS of HUVECs, to serve as a visual indicator of the cellular oxidative stress level. As shown in Fig. 6d, after being incubated in a high concentration H_2O_2 environment, the HUVECs exhibited bright green fluorescence, indicating its high intracellular ROS level. After the introduction of CF–cur hydrogel or CF–CuS–cur hydrogel in the cell culture

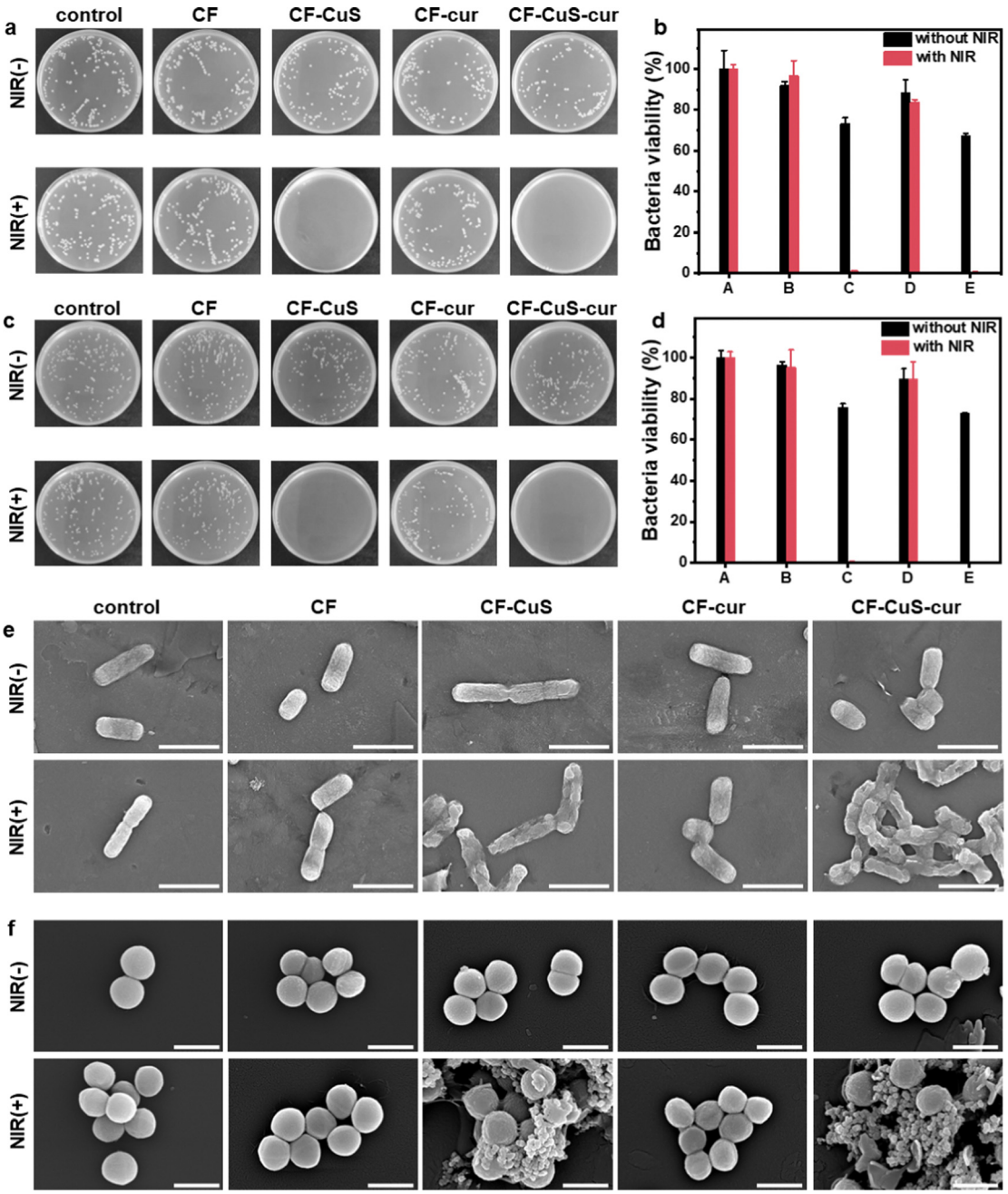

Fig. 5 Representative bacterial colony images of (a) *E. coli* and (c) *S. aureus* after various treatments, with the corresponding statistical bacteria viability of (b) *E. coli* and (d) *S. aureus*, (A) control, (B) CF hydrogel, (C) CF–CuS hydrogel, (D) CF–cur hydrogel, (E) CF–CuS–cur hydrogel, and the data were expressed as mean ± SDs (n = 3); the SEM images of (e) *E. coli*, scale bar: 2 μm and (f) *S. aureus*, scale bar: 1 μm after various treatments.

medium, the green fluorescence was largely suppressed, demonstrating the effective antioxidant activity of curcumin containing hydrogels. More specifically, in the presence of 400 μM H_2O_2, the HUVECs cell viability dropped to 39.0 ± 2.2%, which can be restored back to 77.5 ± 0.7% and 78.8 ± 0.4% in the presence of CF–cur hydrogel and CF–CuS–cur hydrogel, respectively (Fig. 6e). The above results manifest that CF–CuS–cur hydrogel can scavenge ROS and protect cells from a highly oxidative environment. Moreover, CF–cur hydrogel and CF–CuS–cur hydrogel displayed similar antioxidant activity, as the antioxidant function originates mostly from curcumin.

In vivo wound healing, histological and immunohistochemistry analysis

Sprague Dawley (SD) rats with infected full-thickness cutaneous wounds were selected as the model to evaluate the *in vivo* wound healing ability, and the corresponding hydrogels were applied on the wounds by injection (Fig. S8, ESI†). The wounds (created on day 0) were monitored continuously during the

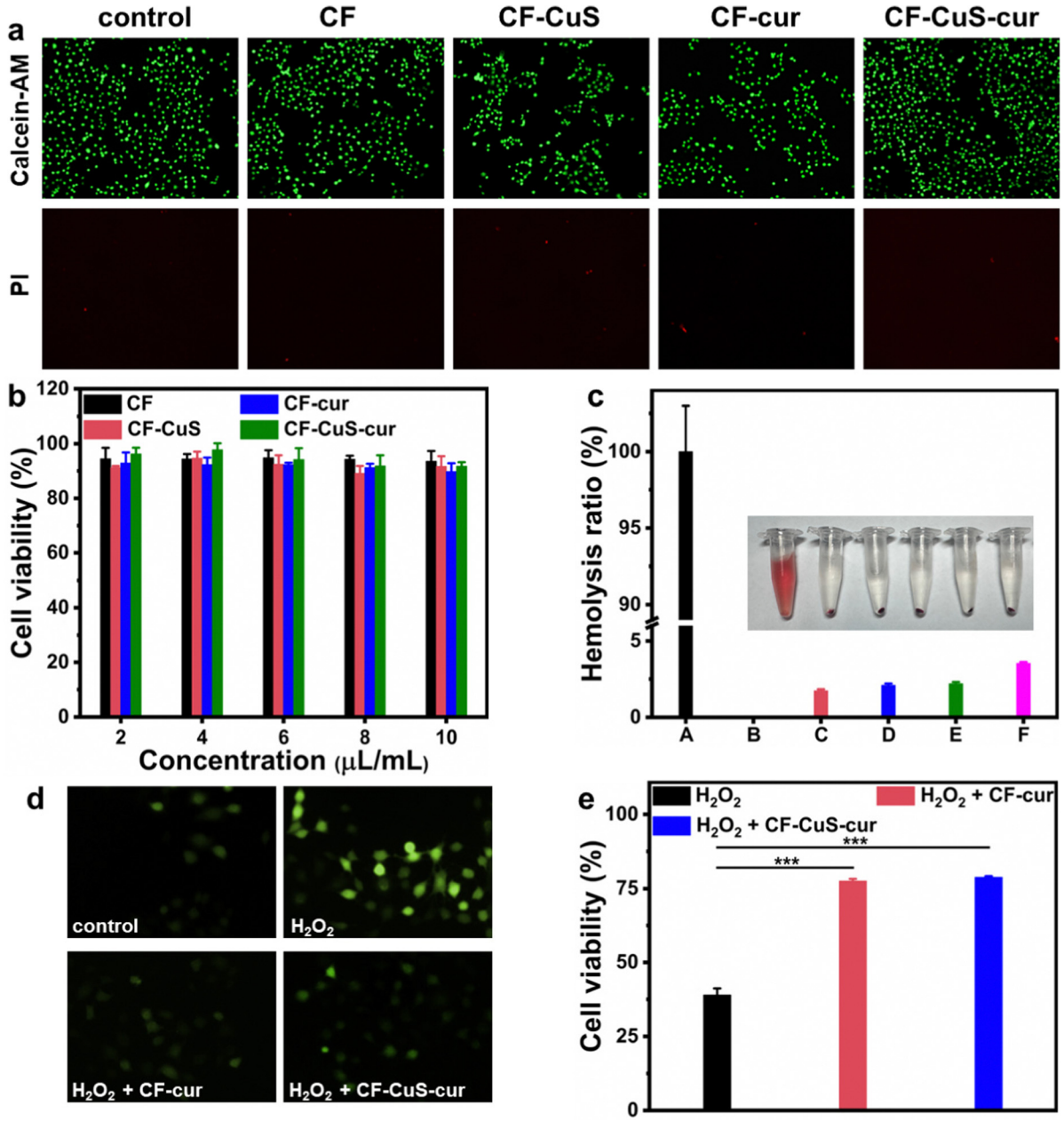

Fig. 6 (a) Calcein-AM/PI live/dead staining of HUVECs after different treatments; (b) viability of HUVECs after being treated with different concentrations of hydrogels, n = 5; (c) the hemolysis assays for different groups, (A) negative control, (B) positive control, (C) CF hydrogel, (D) CF–CuS hydrogel, (E) CF–cur hydrogel, (F) CF–CuS–cur hydrogel; (d) fluorescence images of HUVECs stained with DCFH-DA after different treatments, and (e) the corresponding cell viability data. Data are expressed as mean ± SDs (n = 5). ***$p < 0.001$.

healing stage, and measured on day 3, 7, 11, and 14, respectively. As shown in Fig. 7a, the wounds in CF–CuS hydrogel + NIR and CF–CuS–cur hydrogel + NIR groups healed considerably faster than other experimental groups. More specifically, the wound closure was 47.0 ± 9.3% and 51.8 ± 11.5% on day 3 for CF–CuS hydrogel + NIR and CF–CuS–cur hydrogel + NIR respectively (Fig. 7b), higher than that in the control group (38.7 ± 6.3%), CF hydrogel group (36.1 ± 20.7%), and CF–cur hydrogel group (36.8 ± 0.2%). Throughout the whole wound healing process, CF–CuS–cur hydrogel + NIR group exhibited the best therapeutic effect compared to the other groups with statistical significance, and the wound almost disappeared with wound closure reaching 96.7 ± 0.4% on day 14, whereas the wound closure in the control, CF hydrogel, and CF–cur hydrogel groups was 87.4 ± 0.5%, 88.9 ± 3.8% and 90.4 ± 0.5%, respectively. During the 14 day treatment, the wound area in the CF hydrogel group exhibited a similar change as compared to the control group, indicating its negligible therapeutic effect. Interestingly, CF–cur hydrogel also showed therapeutic effect on day 7 and after to a certain degree. This may result from the intrinsic antibacterial ability of curcumin.[48,49] Moreover, as curcumin has demonstrated an antioxidant property, it may

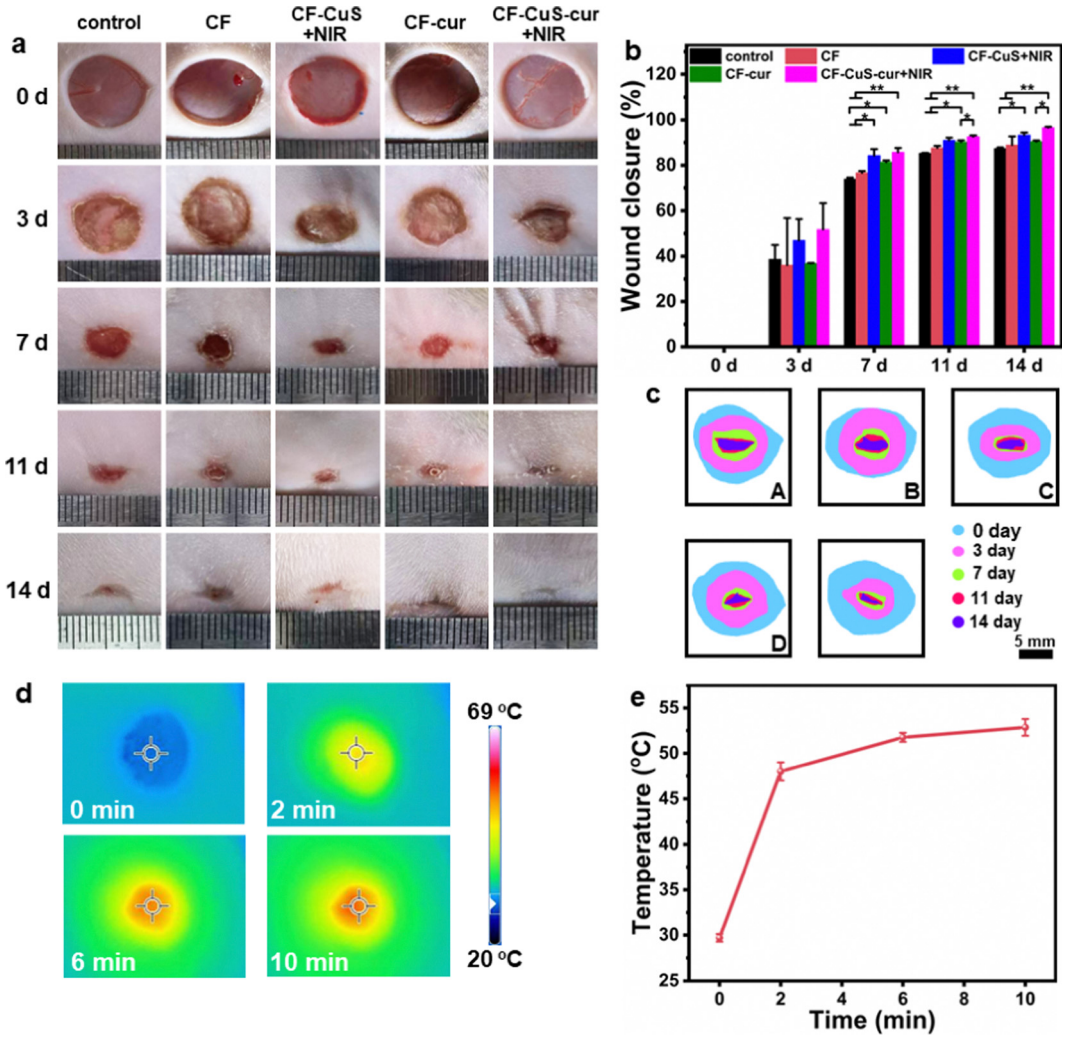

Fig. 7 (a) Representative photographs of infected skin wounds taken on days 0, 3, 7, 11, and 14, in different treatment groups including the control, CF hydrogel, CF–CuS hydrogel + NIR, CF–cur hydrogel, and CF–CuS–cur hydrogel + NIR, where + NIR indicates with NIR irradiation (1064 nm, 0.75 W cm^{-2}, 10 min) on day 0; (b) the corresponding quantification and (c) schematic diagrams of the wound closure with various treatments on day 0, 3, 7, 11, and 14; (d) infrared thermographic images of the wounds surface and (e) the corresponding temporal temperature elevation curve during the NIR irradiation period. Data are expressed as mean ± SDs (n = 3). *$p < 0.05$, **$p < 0.01$.

act positively during the inflammatory period, shorten the inflammation time and promote wound healing. In order to make a better visual comparison between experimental groups, the representative wound area photographed over the treatment time was compiled and digitally redrawn carefully (Fig. 7c). The infrared thermographs shown in Fig. 7d indicates that CF–CuS or CF–CuS–cur hydrogel applied on the wound surface can be heated up quickly under NIR light irradiation after 2–3 min, and reaching a final temperature of 52 °C at the end of the 10 min NIR irradiation period (Fig. 7e), which is sufficient for the photothermal bacteria ablation. However, potential burns may also occur at times, and this calls for the development of effective mild photothermal therapy.

In order to assess the quality of the tissue regeneration at the wound sites, histological analysis (H&E and Masson staining) was conducted using the tissue taken from the wound on day 14. As shown by the H&E staining images in Fig. 8a, there were still broad wound edges in the control and CF hydrogel groups (outlined by the black dotted lines and double-headed arrows), whereas the other three groups displayed relatively narrow edges. The average wound edge of 0.9 ± 0.2 mm for the CF–CuS–cur hydrogel + NIR group is significantly lower than that of the control group (5.0 ± 0.1 mm), CF hydrogel group (4.1 ± 0.1 mm), CF–CuS hydrogel + NIR group (1.8 ± 0.5 mm), and CF–cur hydrogel group (2.1 ± 0.1 mm), with statistical significance $p < 0.001$ (Fig. 8c). Furthermore, the partially enlarged images in Fig. 8a also indicate that there were some skin attachments (pointed by the green arrows) formed in the CF–CuS hydrogel + NIR, CF–cur hydrogel and CF–CuS–cur hydrogel + NIR groups. In addition, Masson staining was used to assess the collagen deposition at the wound sites. As shown in Fig. 8b, CF–CuS hydrogel + NIR and CF–CuS–cur hydrogel + NIR groups displayed the highest amount of collagen deposition (36.9 ± 3.8% and 39.3 ± 3.2%, respectively), compared to

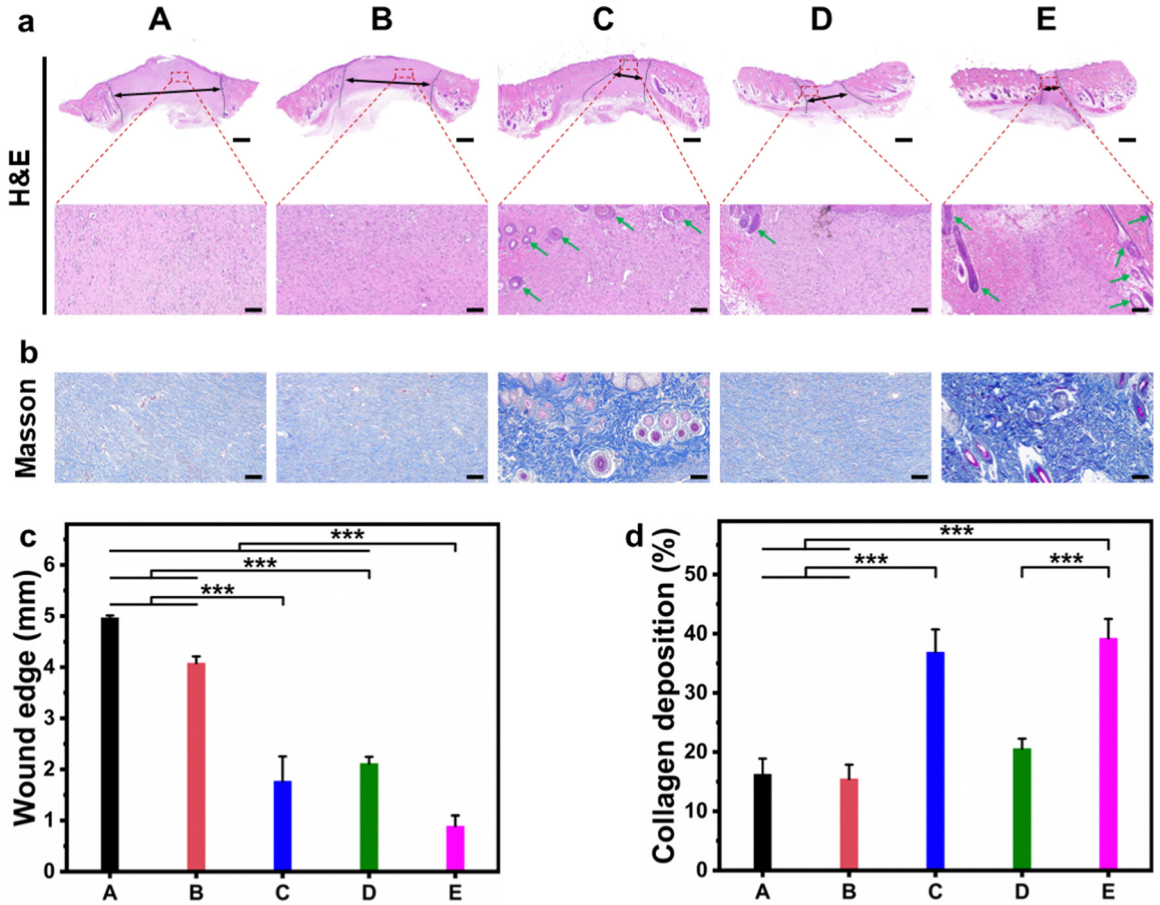

Fig. 8 (a) H&E staining images of the newly formed skin cambium on day 14 (black dotted lines and double-headed arrows depict the wound edge, whereas green arrows point to the skin attachments), scale bar: 1 mm in global images, 0.1 mm in enlarged images; (b) Masson staining images of the newly formed skin cambium on day 14, scale bar: 0.1 mm; the quantitative analysis of (c) wound edge and (d) collagen deposition based on H&E and Masson staining. (A) control, (B) CF hydrogel, (C) CF–CuS hydrogel + NIR, (D) CF–cur hydrogel, and (E) CF–CuS–cur hydrogel + NIR. Data are expressed as mean ± SDs (n = 3). ***$p < 0.001$.

that of the control group (16.2 ± 2.7%), CF hydrogel group (15.5 ± 2.4%), and CF–cur hydrogel group (20.6 ± 1.7%) (Fig. 8d). This could be due to the released Cu^{2+} ions from CuS NPs under NIR light irradiation, which are known to promote fibroblast and vascular endothelial cells proliferation. Combining the above results, we can clearly see that the CF–CuS–cur hydrogel + NIR groups can effectively eliminate bacteria in the infected wounds *via* a photothermal effect, and improve wound closure and collagen deposition by the combined action of Cu^{2+} ions and antioxidant curcumin.

Finally, immunohistochemistry staining of CD31 (Fig. 9a) and CD206 (Fig. 9b) was conducted to evaluate the wound healing process by analyzing the neovascularization degree and macrophage phenotype of the wound tissue. On day 7, neovascularization was significantly facilitated in the CF–CuS hydrogel + NIR, CF–cur hydrogel and CF–CuS–cur hydrogel + NIR groups, indicating that both copper ions and curcumin have a positive effect on neovascularization. Whereas for the control and CF hydrogel groups, rarely any new blood vessels were formed on day 7, which exhibited more CD31 expression on day 14, indicating that the wound repairing stage of these two groups lag behind that of the CF–CuS hydrogel + NIR, CF–cur hydrogel and CF–CuS–cur hydrogel + NIR groups. The different expressions of CD206, which was used to stain M2 macrophages with an anti-inflammatory and wound repairing capacity,[50] also existed among different experimental groups. On day 7, the CF–CuS hydrogel + NIR, CF–cur hydrogel and CF–CuS–cur hydrogel + NIR groups all exhibited significant CD206 expression, corresponding to the predominant M2 macrophage expression, which indicates the wounds were in the final healing and remodeling stage, as the local macrophage population was in the transition to anti-inflammatory M2 macrophage phenotypes. On the other hand, the control and CF hydrogel groups showed very little CD206 expression on day 7, which only emerged to some extent on day 14. This suggests that the wounds were still in the early inflammatory stage on day 7, and only transited to the later wound healing stage during day 7 to 14, for the control and CF hydrogel groups. The combined results of wound sites visual inspection (Fig. 7), histological (Fig. 8) and immunohistochemistry (Fig. 9) analysis demonstrate that CF–CuS–cur hydrogel + NIR treatment facilitated the wound healing process *via* synergistic

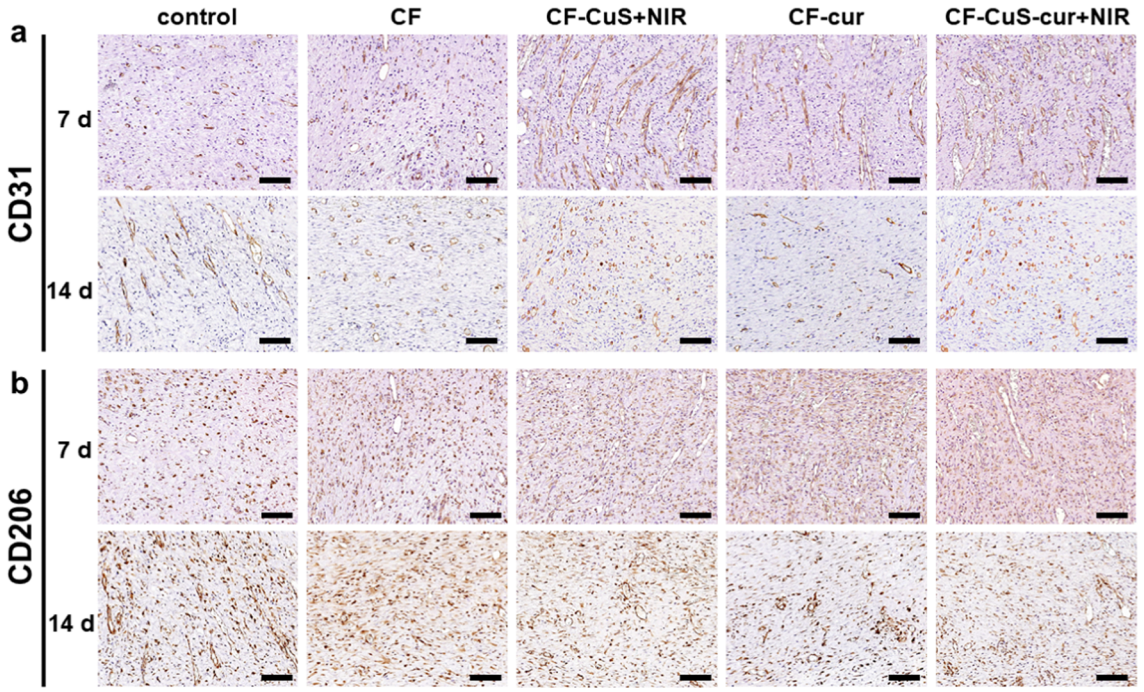

Fig. 9 The immunohistochemistry staining of (a) CD31 and (b) CD206 after 7 and 14 days of various treatments. Scale bar: 0.1 mm.

photothermally enhanced antibacterial activity, promoted collagen deposition and vascular angiogenesis, as well as the antioxidation and anti-inflammation function exerted by curcumin.

By co-loading CuS NPs and curcumin into F127 micelles through an anti-solvent method, adequate dispersion of curcumin in the hydrogel matrix with photothermal-controlled drug releasing capability has been realized, thereby enabling an accelerated wound healing process *via* the synergistic photothermal antibacterial ability of CuS under NIR laser irradiation, and the antioxidant/anti-inflammatory activity from curcumin. However, for their clinical transformations, investigation on the *in vivo* toxicity such as tissue and blood marker analysis[51,52] should be conducted systematically in the future.

Conclusions

In summary, we have prepared CuS NPs and curcumin (cur) co-loaded aldehyde-terminated F127 (F127-CHO@CuS/cur) micelles, which were then cross-linked with carboxymethyl chitosan through a Schiff base reaction, forming a functional composite hydrogel (CF–CuS–cur). The F127-CHO@CuS/cur micelles served as the hydrophobic drug carrier, with NIR light controlled release properties. Apart from the demonstrated appropriate swelling and degradation behavior, injectability to adhere to and cover irregular wounds, and excellent biocompatibility, the CF–CuS–cur hydrogel displayed effective antioxidant and NIR photothermal antibacterial activity due to the co-loaded CuS NPs and curcumin. When the infected full-thickness cutaneous wound was treated with the CF–CuS–cur hydrogel with the assistance of NIR irradiation, the wound healing process was significantly accelerated, due to effective sterilization and decreased inflammation. Histological and immunohistochemistry analysis further confirmed the enhanced wound healing, where the CF–CuS–cur hydrogel with NIR irradiation was revealed to promote skin attachments and regeneration, collagen deposition, neovascularization, and early transition to anti-inflammatory M2 macrophages. The facile strategy to construct functional hydrogels with NIR-enhanced antibacterial and antioxidant properties demonstrated herein may be potentially applied as wound dressings to treat chronic wounds.

Conflicts of interest

There are no conflicts to declare.

Acknowledgements

This work was partially funded by the Suzhou Institute of Nanotech and Nano-bionics, and by the Six Talent Peaks Project in Jiangsu Province (SWYY-243).

Notes and references

1 T. Liu, Y. Lu, R. Zhan, W. Qian and G. Luo, *Adv. Drug Delivery Rev.*, 2023, **193**, 114670.
2 X. Qu, C. Gao, L. Fu, Y. Chu, J.-H. Wang, H. Qiu and J. Chen, *ACS Appl. Mater. Interfaces*, 2023, **15**, 18608–18619.
3 Y. Liang, Z. Li, Y. Huang, R. Yu and B. Guo, *ACS Nano*, 2021, **15**, 7078–7093.
4 M. Wang, X. Zhou, Y. Li, Y. Dong, J. Meng, S. Zhang, L. Xia, Z. He, L. Ren, Z. Chen and X. Zhang, *Bioact. Mater.*, 2022, **17**, 289–299.

5 S. Mahmoudi, E. Mancini, L. Xu, A. Moore, F. Jahanbani, K. Hebestreit, R. Srinivasan, X. Li, K. Devarajan, L. Prélot, C. E. Ang, Y. Shibuya, B. A. Benayoun, A. L. S. Chang, M. Wernig, J. Wysocka, M. T. Longaker, M. P. Snyder and A. Brunet, *Nature*, 2019, **574**, 553–558.
6 K. Huang, W. Liu, W. Wei, Y. Zhao, P. Zhuang, X. Wang, Y. Wang, Y. Hu and H. Dai, *ACS Nano*, 2022, **16**, 19491–19508.
7 B. Aderibigbe and B. Buyana, *Pharmaceutics*, 2018, **10**, 42.
8 B. Guo, R. Dong, Y. Liang and M. Li, *Nat. Rev. Chem.*, 2021, **5**, 773–791.
9 H. Zhao, J. Huang, Y. Li, X. Lv, H. Zhou, H. Wang, Y. Xu, C. Wang, J. Wang and Z. Liu, *Biomaterials*, 2020, **258**, 120286.
10 S. Wang, H. Zheng, L. Zhou, F. Cheng, Z. Liu, H. Zhang, L. Wang and Q. Zhang, *Nano Lett.*, 2020, **20**, 5149–5158.
11 L. Zhou, F. Chen, Z. Hou, Y. Chen and X. Luo, *Chem. Eng. J.*, 2021, **409**, 128224.
12 P. Jia, Y. Zou and J. Jiang, *ACS Appl. Mater. Interfaces*, 2023, **15**, 22929–22943.
13 Y. Kong, Z. Hou, L. Zhou, P. Zhang, Y. Ouyang, P. Wang, Y. Chen and X. Luo, *ACS Biomater. Sci. Eng.*, 2021, **7**, 335–349.
14 M. Li, X. Liu, L. Tan, Z. Cui, X. Yang, Z. Li, Y. Zheng, K. W. K. Yeung, P. K. Chu and S. Wu, *Biomater. Sci.*, 2018, **6**, 2110–2121.
15 J. Wang, H. Cheng, W. Chen, P. Han, X. Yao, B. Tang, W. Duan, P. Li, X. Wei, P. K. Chu and X. Zhang, *Chem. Eng. J.*, 2023, **452**, 139474.
16 Y. Qiao, Y. Ping, H. Zhang, B. Zhou, F. Liu, Y. Yu, T. Xie, W. Li, D. Zhong, Y. Zhang, K. Yao, H. A. Santos and M. Zhou, *ACS Appl. Mater. Interfaces*, 2019, **11**, 3809–3822.
17 L. Wang, Z. Hussain, P. Zheng, Y. Zhang, Y. Cao, T. Gao, Z. Zhang, Y. Zhang and R. Pei, *J. Mater. Chem. B*, 2023, **11**, 2166–2183.
18 K.-H. Shen, C.-H. Lu, C.-Y. Kuo, B.-Y. Li and Y.-C. Yeh, *J. Mater. Chem. B*, 2021, **9**, 7100–7116.
19 M. L. Ermini and V. Voliani, *ACS Nano*, 2021, **15**, 6008–6029.
20 M. Zong, L. Bai, Y. Liu, X. Wang, X. Zhang, X. Huang, R. Hang and B. Tang, *Mater. Sci. Eng., C*, 2017, **71**, 93–99.
21 K. L. Worthington, A. Adamcakova-Dodd, A. Wongrakpanich, I. A. Mudunkotuwa, K. A. Mapuskar, V. B. Joshi, C. Allan Guymon, D. R. Spitz, V. H. Grassian, P. S. Thorne and A. K. Salem, *Nanotechnology*, 2013, **24**, 395101.
22 T. Liu, B. Xiao, F. Xiang, J. Tan, Z. Chen, X. Zhang, C. Wu, Z. Mao, G. Luo, X. Chen and J. Deng, *Nat. Commun.*, 2020, **11**, 2788.
23 Y. Peng, D. He, X. Ge, Y. Lu, Y. Chai, Y. Zhang, Z. Mao, G. Luo, J. Deng and Y. Zhang, *Bioact. Mater.*, 2021, **6**, 3109–3124.
24 X. Li, Y. Liu, X. Qi, S. Xiao, Z. Xu, Z. Yuan, Q. Liu, H. Li, S. Ma, T. Liu, Y. Huang, X. Zhang, X. Zhang, Z. Mao, G. Luo and J. Deng, *Adv. Mater.*, 2022, **34**, 2109004.
25 X. He, X. Liu, J. Yang, H. Du, N. Chai, Z. Sha, M. Geng, X. Zhou and C. He, *Carbohydr. Polym.*, 2020, **247**, 116689.
26 Z. Liu, X. Chen, W. Ma, Y. Gao, Y. Yao, J. Li, T. Zhang, X. Qin, Y. Ge, Y. Jiang and Y. Lin, *Adv. Funct. Mater.*, 2022, **32**, 2204587.
27 J. Liu, Z. Chen, J. Wang, R. Li, T. Li, M. Chang, F. Yan and Y. Wang, *ACS Appl. Mater. Interfaces*, 2018, **10**, 16315–16326.
28 C. Mohanty and S. K. Sahoo, *Drug Discovery Today*, 2017, **22**, 1582–1592.
29 B. Hu, M. Gao, K. O. Boakye-Yiadom, W. Ho, W. Yu, X. Xu and X. Q. Zhang, *Bioact. Mater.*, 2021, **6**, 4592–4606.
30 M. di Luca, M. Curcio, E. Valli, G. Cirillo, F. Voli, M. E. Butini, A. Farfalla, E. Pantuso, A. Leggio, F. P. Nicoletta, A. Tavanti, F. Iemma and O. Vittorio, *J. Mater. Chem. B*, 2019, **7**, 4361–4370.
31 B. Joe, M. Vijaykumar and B. R. Lokesh, *Crit. Rev. Food Sci. Nutr.*, 2004, **44**, 97–111.
32 R. Jäger, R. P. Lowery, A. V. Calvanese, J. M. Joy, M. Purpura and J. M. Wilson, *Nutr. J.*, 2014, **13**, 11.
33 P. Anand, A. B. Kunnumakkara, R. A. Newman and B. B. Aggarwal, *Mol. Pharmaceutics*, 2007, **4**, 807–818.
34 K. Fang, R. Wang, H. Zhang, L. Zhou, T. Xu, Y. Xiao, Y. Zhou, G. Gao, J. Chen, D. Liu, F. Ai and J. Fu, *ACS Appl. Mater. Interfaces*, 2020, **12**, 52307–52318.
35 A. V. Kabanov, E. V. Batrakova and V. Y. Alakhov, *J. Controlled Release*, 2002, **82**, 189–212.
36 J. Xu, K. Wang, Y. Li, Y. Li, B. Li, H. Luo, H. Shi, X. Guan, T. Zhang, Y. Sun, F. Chen, H. He, J. Zhang, L. Cai, W. Song, J. Wu and X. Li, *Chem. Eng. J.*, 2023, **454**, 140027.
37 S. Li, C. Yang, J. Li, C. Zhang, L. Zhu, Y. Song, Y. Guo, R. Wang, D. Gan, J. Shi, P. Ma, F. Gao and H. Su, *Int. J. Nanomed.*, 2023, **18**, 4485–4505.
38 B. Yang, J. Song, Y. Jiang, M. Li, J. Wei, J. Qin, W. Peng, F. L. Lasaosa, Y. He, H. Mao, J. Yang and Z. Gu, *ACS Appl. Mater. Interfaces*, 2020, **12**, 57782–57797.
39 J. Qu, X. Zhao, Y. Liang, T. Zhang, P. X. Ma and B. Guo, *Biomaterials*, 2018, **183**, 185–199.
40 K. Liu, L. Liu, H. Guo, R. Xu, X. Liang, Y. Chen, H. Li, X. Fu, X. Wang, H. Chen, Y. Li and J. Yang, *Adv. Healthcare Mater.*, 2023, **12**, 2202010.
41 X. Zhang, J. Feng, W. Feng, B. Xu, K. Zhang, G. Ma, Y. Li, M. Yang and F. J. Xu, *ACS Appl. Mater. Interfaces*, 2022, **14**, 31737–31750.
42 M. Liu, X. Xue, C. Ghosh, X. Liu, Y. Liu, E. P. Furlani, M. T. Swihart and P. N. Prasad, *Chem. Mater.*, 2015, **27**, 2584–2590.
43 N. Gao, S. Lü, C. Gao, X. Wang, X. Xu, X. Bai, C. Feng and M. Liu, *Chem. Eng. J.*, 2016, **287**, 20–29.
44 G. Chang, Q. Dang, C. Liu, X. Wang, H. Song, H. Gao, H. Sun, B. Zhang and D. Cha, *Carbohydr. Polym.*, 2022, **292**, 119687.
45 W. Nie, Y. Huang, Y. Wang, C. Kengla, J. Scott Copus, J. Sun, Z. Shao, X. Dai and Y. Shen, *Chem. Eng. J.*, 2022, **446**, 136948.
46 R.-S. Juang, K.-S. Wang, Y.-W. Cheng, W.-E. Wu, Y.-H. Lin, R.-J. Jeng, L.-Y. Huang, M.-C. Yang, S.-H. Liu and T.-Y. Liu, *Spectrochim. Acta, Part A*, 2022, **279**, 121475.
47 Y. Liang, X. Zhao, T. Hu, B. Chen, Z. Yin, P. X. Ma and B. Guo, *Small*, 2019, **15**, 1900046.
48 S. Y. Teow, K. Liew, S. A. Ali, A. S. Khoo and S. C. Peh, *J. Trop. Med.*, 2016, **2016**, 2853045.

49 Y. Wu, K. Wang, Q. Liu, X. Liu, B. Mou, O. M. Lai, C. P. Tan and L. Z. Cheong, *Food Chem.*, 2022, **367**, 130700.
50 Z. Hao, G. Liu, L. Ren, J. Liu, C. Liu, T. Yang, X. Wu, X. Zhang, L. Yang, J. Xia and W. Li, *ACS Appl. Mater. Interfaces*, 2023, **15**, 19847–19862.
51 R. Shi, H. Li, X. Jin, X. Huang, Z. Ou, X. Zhang, G. Luo and J. Deng, *Acta Biomater.*, 2022, **152**, 425–439.
52 D. He, T. Yang, W. Qian, C. Qi, L. Mao, X. Yu, H. Zhu, G. Luo and J. Deng, *Appl. Mater. Today*, 2018, **12**, 415–429.